RGNZ/MGPB

Empirical equation for predicting fracture frequency of carbonate and silicate rocks using P-wave velocity

Rudarsko-geološko-naftni zbornik
(The Mining-Geology-Petroleum Engineering Bulletin)
DOI: 10.17794/rgn.2025.3.3

Original scientific paper

Sari Melati[1,2], Ridho K. Wattimena[1], David P. Sahara[1*], Ganda M. Simangunsong[1], Wahyu Hidayat[1,3]

[1] *Faculty of Mining and Petroleum Engineering, Institut Teknologi Bandung, Bandung 40132, Indonesia.*
[2] *Faculty of Engineering, Universitas Lambung Mangkurat, Banjarbaru 70714, Indonesia.*
[3] *Faculty of Technology Mineral, UPN Veteran, Yogyakarta 55283, Indonesia.*

Abstract

Fracture frequency (FF) is necessary for fracture quantification in rock mass classification systems and plays an important role in the mechanical properties of rock mass. To date, laboratory studies on the effects of jointed rock on rock velocity have been limited to high FF conditions and have not incorporated lithological variations. This study aimed to estimate the FF indirectly by determining its relationship with wave velocity in carbonate and silicate rocks. Two carbonate (CA1 and CA2) and two silicate (CR1 and CR2) rocks were drilled from four sites on the Java Island in Indonesia, and their characteristics were identified through petrographic tests, physical property measurements, and ultrasonic velocity tests. Artificial joints were made in the core samples of these rocks to create varying joint spacing, especially at low frequencies between 0 and 24 joints per metre. We successfully obtained new empirical equations expressing the relationship among the FF, intact rock P-wave velocity (Vp_o), and jointed rock P-wave velocity (Vp_j). For CA1, CA2, CR1, and CR2, the Vp_j/Vp_o ratios were 1–0.0172FF, 1–0.0301FF, 1–0.0371FF, and 1–0.0349FF, respectively. The coefficient of determination of the equation for each lithology showed that the porosity, velocity, and density affected the fitting of the data to the equation. Overall, the findings of this study can be used to optimise the utilisation of geophysical methods for geotechnical monitoring, especially the identification of FF in lithology contrast between carbonate and silicate rocks or rocks with different compaction levels.

Keywords:
carbonate, silicate, fracture frequency, ultrasonic measurement, rock velocity

1. Introduction

Fracture frequency is one of the indicators for determining the rock mass class and the geotechnical properties of rock mass on site (**Laubscher, 1990; Sen, 2014; Sen and Sadagah, 2003**). In the exploration stage, fracture frequency data are usually obtained from direct joint measurements on rock core samples (**Higgs, 1984; He et al., 2021; Khorzughi et al., 2018; Panek, 1984**). Indeed, this method requires heavy funding and a long time for core drilling. In the production operation stage, fracture frequency data can be obtained by directly measuring the exposed rock mass in surface excavation and underground space (**Sriwidada and Kurnia, 2017; Gumede and Stacey, 2007; Kim and Song, 2019; Priest, 2004**). However, the condition of the unexposed rock mass is also disturbed by the excavation that is not covered in the mapping range. Therefore, an indirect method is required to predict the fracture frequency affected by excavation, thereby enabling a wider spatial coverage.

Given the presence of joints in the rock mass and fracture frequency in the field impact wave propagation (**Varma, et al., 2021; Moos and Zoback, 1983**), there is an opportunity to quantify the relationship between the fracture frequency and wave velocity through laboratory experiments. The characteristics of velocity changes are expected to be understood through direct laboratory measurements of rock samples representing rock mass in fields. Estimating the fracture frequency from geophysical information of wave velocity can be very valuable if a conversion method to link it exists.

In addition to fracture frequency, rock lithology is an important factor that must be understood in engineering identification at project sites (**Matula, 1969; Marinos et al., 2019; Mandrone, 2006**). Oil and gas deposits are often formed by the migration of sedimentary carbonate rocks through heterogeneous sedimentary lithologies (**Ahr, 2011; Zhou et al, 2020**). Moreover, mineralised zones are often formed in carbonate rocks penetrated by

* Corresponding author: David P. Sahara
e-mail address: david_sahara@itb.ac.id
Received: 25 October 2024. Accepted: 17 January 2025.
Available online: 3 July 2025

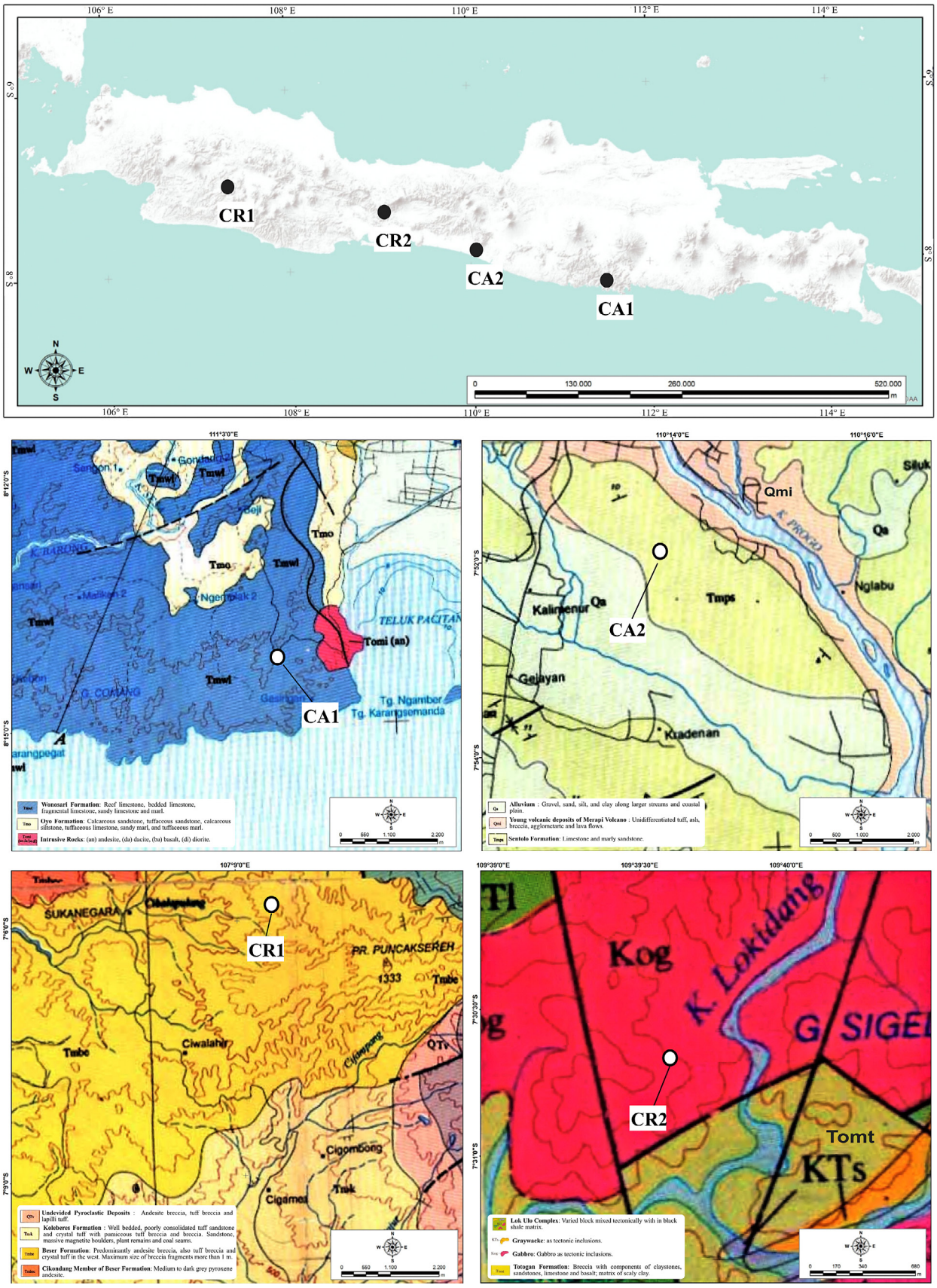

Figure 1. Drilling locations of rock samples from Java Island. CA1: Limestone from Wonosari Formation, East Java. CA2: Limestone from Sentolo Formation, Yogyakarta. CR1: Andesite from Beser Formation, West Java. CR2: Gabbro from Mount Parang, Central Java (modified from **Samodra et al., 1992**; **Rahardjo et al., 1995**; **Koesmono et al., 1996**; **Asikin et al., 1992**)

magma or bordered by igneous rocks (**Pollard, 2005; Dugdale et al., 2009; Voudouris et al., 2008**) such as skarn deposits, which are mined massively by underground mining methods (**Brannon et al., 2020**).

An empirical equation model expressing the relation between fracture frequency and P-wave velocity was previously developed using ultrasonic velocity measurement on drill core samples in the laboratory (**Kurtulus et al., 2012; Huang et al, 2014; Leucci and De Giorgi, 2006; Varma et al, 2017**). Artificial fractures in the tested sample approached those in the rock mass model with varying fracture spacing. However, the sample size and fracture spacing remained limited. The dimensions of the samples examined in these studies ranged from 0.6 m with a maximum of 7 joints to 0.2 cm with a maximum of 3 joints. Thus, these studies examined the effect of fracture spacing on fracture frequencies of more than 6.67 joints per metre, which is equivalent to poor or very poor rock mass. As a result, these studies are less relevant for application to rock mass classes with a smaller fracture frequency range, which represent a more competent rock mass.

Microseismic monitoring has been widely applied in underground mines (**Cai et al., 2014; Wang et al., 2018, Hidayat et al., 2024; Qian et al, 2018**) for seismic hazard assessment and velocity mapping. Seismic tomography is commonly used to map the seismic wave velocity near an excavation zone. Seismic tomography can be optimised by understanding the characteristics of V_p and fracture frequency in heterogeneous lithologies. In addition to in situ fracture identification, seismic tomography can potentially aid in monitoring crack propagation due to the use of hydraulic fracturing in oil production well drilling activities or rock mass preconditioning in underground mines (**Martyushev et al., 2024; Cordova et al., 2023**).

This study aimed to build empirical equations for monitoring velocity changes upon transitioning from competent rock mass to fractured rock mass. Ultrasonic velocity measurements were performed with joint densities ranging from 0 to 24 joints/metre. Owing to the availability of long samples from four sites, our study objective was feasible. In addition to the joint density scale, we also analysed the influence of rock lithology. Carbonate and silicate rocks were measured to determine the impact of different lithological characteristics on velocity changes due to fracture frequency variations and optimise their use in heterogeneous rocks. The empirical equations obtained in this study can be used for geotechnical monitoring using seismic velocity, especially for the identification of fracture frequency in different lithology.

2. Materials and methods

2.1. Location of core drilling

The rock samples tested in this study consisted of carbonate sedimentary rocks and silicate igneous rocks. We conducted core drilling on rock samples on Java Island, Indonesia. Java Island is on the southern edge of the Southeast-Asian plate, bordering the Indo-Australian plate that is inclined to the north. This geological setting causes Java Island to be tectonically active, as evidenced by geomorphic indicators in the form of living and raised coral reefs, volcanoes, and fault scarps (**Verstappen, 2010**). The genesis of rocks on Java Island is related to the activity of quaternary plates and sedimentation process; thus, carbonate and silicate rocks are formed on this island. The location of sample drilling is presented on the map in **Figure 1**. The detailed location of each formation is indicated in geological maps. The samples were selected as representatives of carbonate rocks and silicate (igneous) rock samples so that this study could cover the heterogeneity of lithology.

The first carbonate rock sample CA1 is limestone from the Wonosari Formation, Pacitan, East Java. The Wonosari Formation is dated to the Middle to Late Miocene, or approximately 5 to 16 million years ago (**Wibowo et al., 2023**). The Wonosari Formation comprises layered and reef limestone. The second carbonate rock sample CA2 is the limestone obtained from the Sentolo Formation, Yogyakarta. The Sentolo Formation is dated to the Middle to Late Miocene (12 – 22 million years ago) (**Akmaluddin and Agustin, 2019**). These carbonate rock samples, CA1 and CA2, were studied to represent typical carbonate rocks that were often on hydrocarbon, hydrothermal, or geothermal traps.

The first igneous rock sample CR1 is an andesite rock from the Beser Formation, West Java. The Beser Formation is the oldest volcanic rock unit in West Java. The Beser Formation can be dated to late Pliocene, or approximately 1.8 – 3.6 million years ago (**Haryanto and Sudjradjat, 2018**). The second igneous rock sample CR2 is a Gabbro rock from Mount Parang in the Karang Sambung Formation, Central Java. Mount Parang is a tertiary volcanic rock interpreted as an intrusion. Gabbro, also called Diabase, from Mount Parang, is estimated to be 26–39 million years old, and is dated to Eocene–Oligocene transition (**Mareta et al., 2020**). Both silicate rock samples, CR1 and CR2, represent typical rocks found in the mineralized zones found in ore mines.

2.2. Sample characterisation

The four drill cores were petrophysically tested to understand the characteristics of the samples and perform their rock velocity analysis. The petrophysical parameters tested in the laboratory were density and porosity because these two parameters were closely related to the velocity of seismic waves passing through the rock mass. Porosity, density, and velocity are indicators of the compaction rate of rocks. The samples were then prepared into thin sections to identify their mineral content and rock petrology characteristics. The percentage of mineral composition was determined by calculating the interpretation of mineral distribution in sections using

the point counting technique. The mineral present at each examined point was identified, the occurrences of each mineral were counted across a set number of points. The percentage of each mineral was calculated by comparing its count to the total number of points examined. This information was used as a reference for the mineralogical characteristics of the rock and its rock velocity.

2.3. Sample preparation

Advanced measurements were utilised to accurately measure the wave velocity of jointed rocks. Fractured sample models were prepared using a diamond rock cutter from irregular core drilling samples into samples cut across the axis of the borehole. The purpose was to measure the fracture frequency range from 0 to 24 joints per metre. The spacing between artificial joints and the cutting planes of the rock samples were arranged in various configurations and calculated as the number of joints per metre. For example, to obtain a sample with a fracture frequency of 2 joints per metre, three core pieces of approximately 30–40 cm length were arranged in parallel. The length of the prepared sample was adjusted to the available core fragments. **Figure 2** presents several examples of rock-cutting configurations to obtain varying fracture frequencies. The surfaces of the cut rock sample planes were smoothened using sandpaper to achieve uniform roughness of the joints, so that identically smooth surfaces can be obtained for planar joints. Vaseline was applied to the surface of the joints to assist in the propagation of waves passing through joints.

The existing joint and/or fractures in the core sample were not taken into account when creating the artificial joint. The variation in the direction and surface roughness of existing joints or fractures was difficult to control as an independent parameter in this study. Fractions of core samples were sorted visually. Only intact drill core fractions were selected to make artificial joints in order to ensure that the measured wave velocity difference would actually occur because of the variation in joint space.

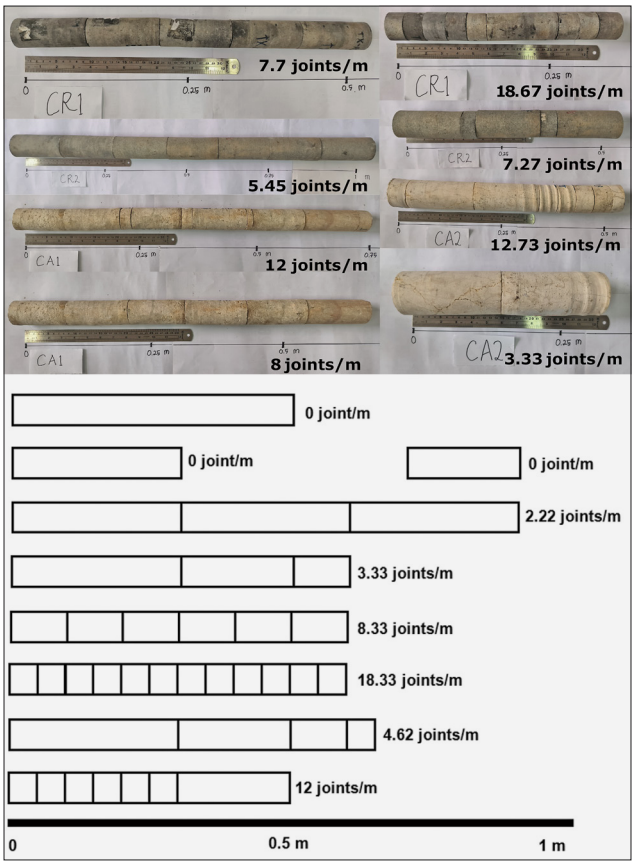

Figure 2. Photo and illustration of certain examples of sample configuration to obtain fracture frequency variation. Fracture frequency is calculated by dividing the number of fractures by the total length of the sample.

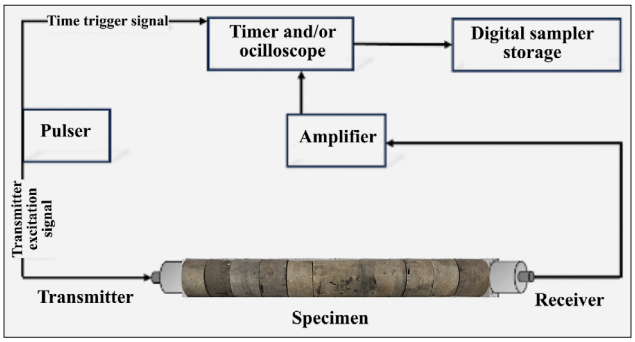

Figure 3. A simplified diagram illustrating the fundamental elements of an ultrasonic apparatus. This study transformed a group of rock cores into jointed rock samples with a total sample length ranging from 0.3 to 1 m. The cores were cut perpendicular to their axis to create artificial joints using a rock cutter to form parallel joints.

2.4. Ultrasonic velocity measurement

Ultrasonic velocity measurements using sound waves with frequencies above 20 kHz were conducted to test the impact of fracture frequency on variations in the wave velocity in rock samples. Following the International Society of Rock Mechanics (ISRM)'s suggested method for determining sound velocity through the ultrasonic pulse transmission technique, a series of standard tests were performed (**Ullusay, 2015**). The testing was conducted using Sonic Viewer Oyo 2i in the Geophysical Instrumentation and Rock Characterization Laboratory in Institut Teknologi Bandung.

In the experimental procedure, the specimen was carefully positioned between two transducers with identical characteristics (see **Figure 3**). A high-voltage pulse was then applied to one of these transducers, which generated ultrasonic waves. These waves propagated through the specimen and were captured by another set of transducers designed specifically for receiving them. The frequency range used in this setup included P-200 kHz and S-100 kHz transducers, chosen specifically for measuring jointed rock samples. An ultra-high-speed A/D converter captured waveform data from the received waves to accu-

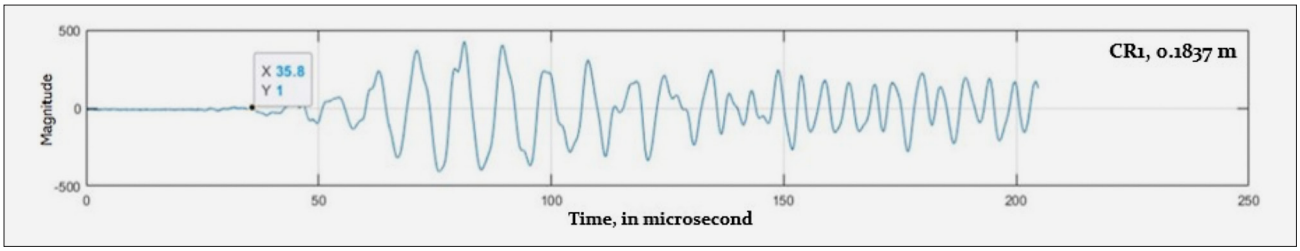

Figure 4. Recorded P waves from rock samples. The arrival times of these waves are indicated by black dots marking the picking point.

rately measure propagation time. These data could be visualised on a display as waveform patterns. Analysing these patterns with precision made it possible to determine propagation times with great accuracy.

In this study, all artificial joints were made in the direction transverse to the axis of the drill core because the orientation of the fracture affected the wave velocity, where the greatest deceleration occurred in fractures perpendicular to the direction of wave propagation. Therefore, the relationship obtained from these measurements considers the differences in natural fracture orientation that might occur in the rock mass. Waveforms from 170 measurements of intact and fractured rock samples were analysed to determine the wave arrival times. These waves were analysed using the Sonic Viewer software to record their time function, with wave arrival times determined by identifying the first break on waveform visualisations (an example of wave travel time determination is shown in **Figure 4**). Wave velocity was measured and calculated using **Equation 1**.

$$\mathrm{Vp} = \frac{L}{T_p} \tag{1}$$

Where:

V_p – the P-wave velocity of measured sample (km/s),
L – the total length of the measured sample (km),
T_p – the travel time of ultrasonic P-wave (s).

The V_p values were plotted on a graph to show the distribution pattern of the relationship with fracture frequency. Fracture frequency (sometimes called joint number or crack density) was quantified in the number of joints per metre. The fracture frequency (FF) was calculated using **Equation 2**.

$$\mathrm{FF} = \frac{J_n}{L} \tag{2}$$

Where:

FF – the fracture frequency (m^{-1}),
Jn – the *number* of joints in sample configurations (joints),
L – total *length* of the measured sample (m).

2.5. Construction of empirical equations

The relationship between FF and V_p was examined using empirical equations tailored to different lithology types. The linear correlation model, its equation, and the coefficient of determination (R^2) for each lithology and rock group were analysed. **Equation 3** is an empirical linear equation model obtained from experimental tests in the laboratory. Vp_j/Vp_0 is the ratio between the fractured sample and intact sample's wave velocity. The FF multiplier coefficient in empirical equation A indicated the degree of influence of FF on the change of P waves. The greater the value of A, the easier the FF reduced the wave velocity in fractured rocks. R^2 was utilised to evaluate the reliability of the equations because it described the accuracy of the data on the predicted value of the equation (**Lee Rodgers and Nicewander, 1988; Taraldsen, 2021**). The correlation relationship between parameters in the data and the equation was described by coefficient r, i.e. the root of R^2 (see **Table 1**).

$$\frac{Vp_j}{Vp_0} = 1 - AFF \tag{3}$$

Where:

Vpj – the P-wave velocity of jointed sample (km/s),
Vp0 – the P-wave velocity of intact sample (km/s),
A – the coefficient of decrease,
FF – the fracture frequency (m^{-1}).

Table 1. Interval of coefficient of determination, coefficient of correlation, and its description (**Lee Rodgers and Nicewander, 1988**)

Coefficient of determination (R^2)	Coefficient of correlation (r)	Description
0.00 – 0.36	0.00 – 0.19	Very weak
0.04 – 0.15	0.20 – 0.39	Weak
0.16 – 0.35	0.40 – 0.59	Moderate
0.36 – 0.62	0.60 – 0.79	Strong
0.64 – 1.00	0.80 – 1.00	Very strong

3. Results and discussion

3.1. Petrophysical and mineralogical characteristics

A set of core samples of hard rock was prepared for the measurement. As shown in **Figure 5**, sample CA1 has the lowest P-wave velocity (3.37 km/s) and the high-

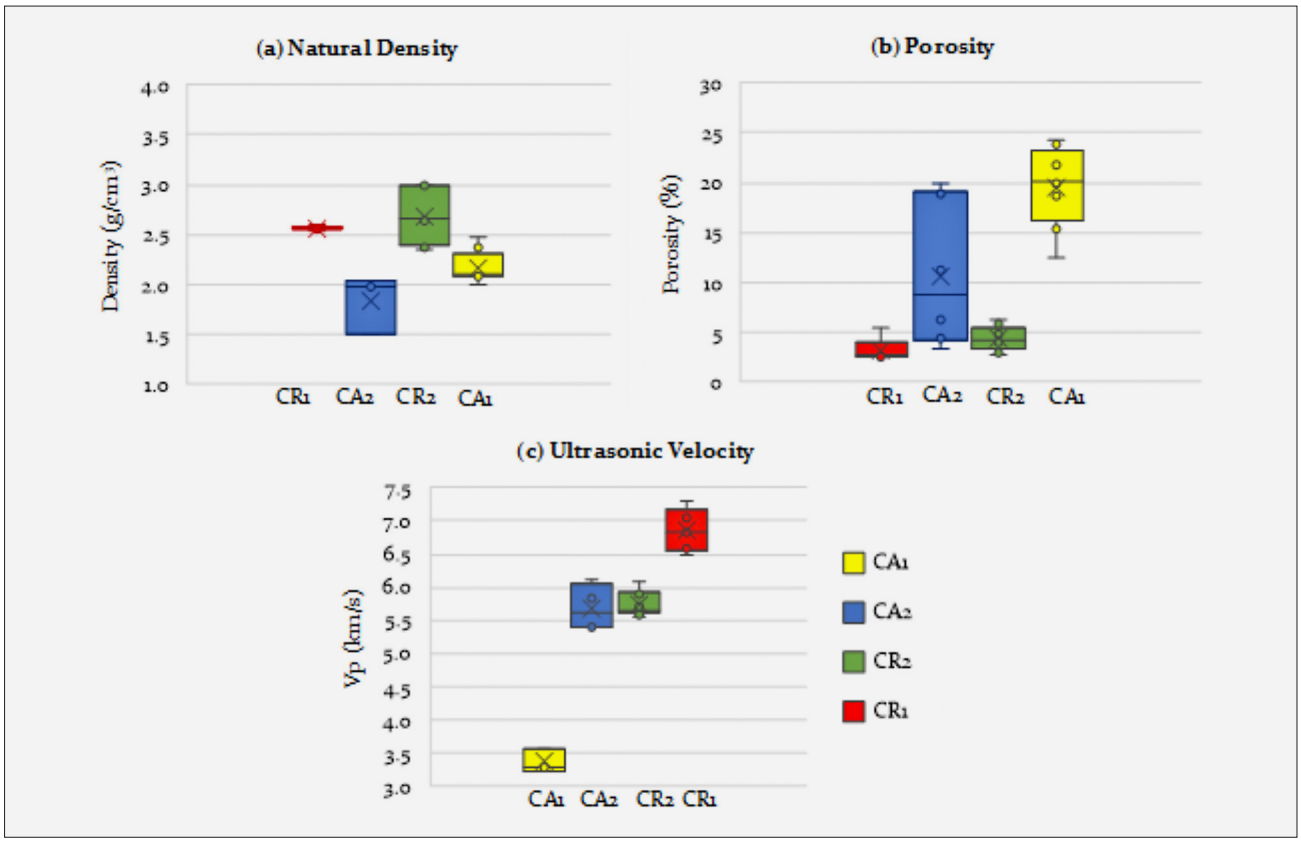

Figure 5. Physical and dynamic properties of samples: (a) natural density (in g/cm³), (b) porosity (in %), and (c) ultrasonic velocity (in km/s).

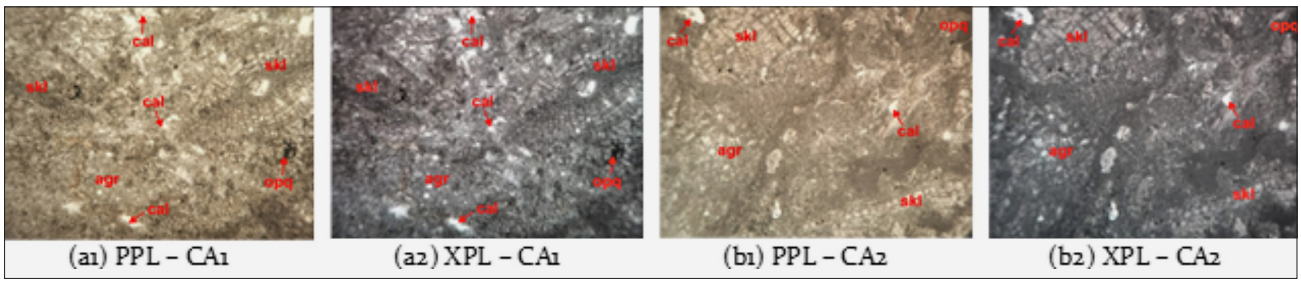

Figure 6. Petrograph of thin sections of carbonate rocks captured under parallel polarisation light (PPL) and cross-polarisation light (XPL): (a1 and a2) CA1 – Wonosari Limestone, and (b1 and b2) CA2-Sentolo Limestone. Abbreviations in figure: skl, Skeleton; cal, Calcite; opq, Opaque minerals; arg, Grain aggregate.

est porosity (21.04%). Sample CA2 has average V_p, density, and porosity values of 5.91 km/s, 2.43 g/cm^3, and 4.44%, respectively. CR1 has the highest average V_p and density of 6.6 km/s and 2.9 g/cm^3, respectively. CR2 has average Vp, density, and porosity values of 5.64 km/s, 2.59 g/cm^3, and 4.43%, respectively.

The prepared CA1, CA2, CR1, and CR2 samples have average natural densities of 2.11, 2.43, 2.90, and 2.59 g/cm^3, and porosities of 21.04%, 4.44%, 4.90%, and 4.43%, respectively. The rock velocity increases in the order CA1 < CR2 < < CA2 < CR1. Evidently, silicate igneous rocks (CR1 and CR2) with high density and relatively lower porosity have relatively higher ultrasonic velocities, namely 6.60 and 5.64 km/s, respectively. While CA2 has the lowest ultrasonic velocity, i.e. 3.37 km/s, it also has the lowest natural density, with porosity up to nearly 21%. As for CA2, its velocity is almost the same as that of CR2, with a density of more than 2.4 g/cm^3 and porosity less than 5%. In general, the results of petrophysical characteristic tests provide a fairly consistent pattern suggesting that rock velocity will be high if density and porosity are low. This aligns with the results of previous studies on calcarenite rock samples conducted by **Rahmouni et al. (2013)**.

3.1.1. Carbonate rocks

The bioclast and matrix have been identified on thin sections with a polarisation microscope under parallel polarisation light (PPL) and cross-polarisation light to

determine the rock name. The following subsections explain the petrography of two carbonate rock samples (shown in **Figure 6**).

3.1.1.1. CA1

CA1 was the first limestone sample drilled from the Wonosari Formation Karts area, Pacitan, Central Java. Thin sections of this carbonate sedimentary rock were brown and clastic in texture and had a grain size less than 0.5–2 mm. The sediment was supported by allochems, subrounded to angular grain shape, poor sorting, and long contact grain. The rock comprised skeletal grains, opaque minerals, aggregate grains, and calcite.

The bioclast and matrix composing Wonosari limestone are indicated in **Figures 6a1** and **6a2** by abbreviations.

- Skeletal foraminifera (25%): brownish white, subrounded grain shape, 2 mm grain size, present centrally, in sections as allochems.
- Skeletal (5%): brownish white, subrounded grain shape, 0.9 mm grain size, present centrally, in sections as allochems.
- Opaque mineral (3%): black, angular grain shape, grain size 0.07 mm, present in a scattered manner.
- Grain aggregate (7%): brownish grey, subrounded grain shape, grain size 1 mm, present in a scattered manner, in sections as allochems.
- Calcite (5%): white, subrounded grain shape, grain size 0.1 mm, present in a scattered manner, in sections as allochems.
- Calcite (45%): brown-black, subrounded grain shape, grain size > 5 microns, present in a scattered manner, in sections as sparite.
- Calcite (10%): brown-black, subrounded grain shape, grain size < 5 microns, present in a scattered manner and abundant in sections as micrite.

The sample was classified as Limestone, based on the mineral identified in this petrography analysis. Its specific rock name was biosparite, according to Folk's classification diagram for gravelly sediment (**Folk, 1959**) or Packstone, according to Dunham's classification system for carbonate sedimentary rocks (**Dunham, 1962**).

3.1.1.2. CA2

CA2 was the second carbonate rock sample drilled from the Sentolo Formation, Kulon Progo, Special Region of Yogyakarta. The thin section was identified as brown carbonate sedimentary rock, clastic texture, grain size less than 0.5–2 mm, supported by allochems, subrounded to angular grain shape, poorly sorted, long contact grain, and composed of skeletal grains, opaque minerals, aggregate grains, and calcite.

The bioclast and matrix composing Sentolo Limestone are indicated in **Figures 6b1** and **6b2**. At first glance, the second sample is similar to the first sample. The difference is the composition of calcite, especially the percentage of micrite, which is more dominant than sparite.

- Calcite (30%); brown-black, subrounded grain shape, grain size < 5 microns, present in a scattered manner and abundant in sections as micrite.
- Grain aggregate (20%): grey-brown, subrounded grain shape, grain size 2 mm, present centrally, in sections as allochems.
- Skeletal (15%): grey, rounded grain shape, grain size 0.9 mm, present centrally, in sections as allochem.
- Calcite (15%): brown-black, subrounded grain shape, grain size > 5 microns, present in a scattered manner in sections as sparite.
- Opaque mineral (7%): black, subrounded grain shape, grain size 0.03 mm, present in a scattered manner.
- Skeletal (5%): colourless, subrounded grain shape, grain size 1.5 mm, present centrally.
- Calcite (8%): white-brown, subrounded grain shape, grain size 0.1 mm, present in a scattered manner.

Based on the mineral content identified in this thin section, the sample was classified as Limestone. The detailed rock name was biomicrite according to Folk's classification diagram for gravelly sediment (**Folk, 1959**), as well as Grainstone, according to Dunham classification system for carbonate sedimentary rocks (**Dunham, 1962**).

Both carbonate rocks tested in this study were of the same rock type, i.e. limestone. However, their texture and grain size were totally different as identified by petrography. Skeletal foraminifera and grain aggregates, i.e. the two main constituents of CA1, had sizes of 2 and 1 mm, respectively. Dominant calcite in CA1 had a grain size >5 microns (sparite), whereas dominant calcite in CA2 had a grain size less than 5 microns (micrite). Skeletal in CA2 had a grain size of 0.9–1.5 mm. Overall, CA1 had a grain texture and CA2 had a fine texture. The genesis and depositional environment of limestone control their difference in compositions and texture. CA1, biosparite, is a limestone composed of calcium carbonate ($CaCO_3$) formed from the remains of marine organisms (such as shells, fossils, and other body parts of organisms) that are fragmented and dispersed in a larger calcium carbonate matrix. Biosparites form in high-energy environments, such as shallow waters, beaches, or coral reefs, where fragments of organisms can collect. In contrast, CA2, biomicrite forms in calm water environments, such as the deep seabed, where fine organic particles can slowly settle. Biomicrite is a limestone formed from fine calcium carbonate derived from the accumulation of small organic fragments or microscopic materials such as the remains of plankton and other microorganisms. The relationship between the composition and tex-

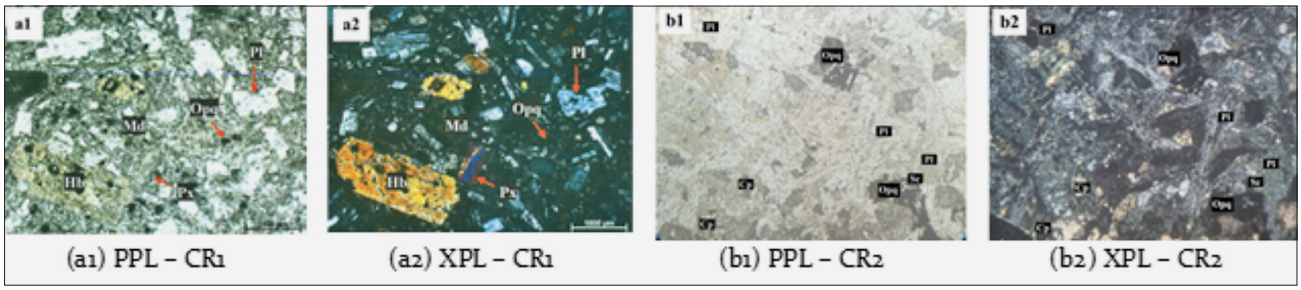

Figure 7. Petrograph under parallel polarisation light (PPL) and cross-polarisation light (XPL) of thin sections: (a1 and a2) CR1, and (b1 and b2) CR2. Abbreviations in figure are: Pl = Plagioclase, Px = Pyroxene, Md = Groundmass, Hb = Hornblende, Opq = Opaque minerals, Cp = Clinopyroxene.

ture from petrography and the physical properties of both limestones can be concluded. Calm water environment tends to deposit biomicrite, a type of limestone with fine texture, high density, and high velocity. Meanwhile, high-energy environment deposits biosparite, a type of limestone that is more porous than biomicrite and has a grain texture.

3.1.2. Silicate rocks

Thin sections of silicate rocks showed all mineral phases that were present in the sample (see **Figure 7**).

3.1.2.1. CR1

CR1 was the first silicate rock sample drilled from the Beser Formation, Baleendah, South Bandung Basin, West Java. The volcanic igneous rock section showed porphyrophanitic texture, holocrystalline, pilotaxitic, massive structure, crystal size less than 0.1 – 3 mm, composed of plagioclase phenocrysts, pyroxene, hornblende, and opaque minerals in a fine-grained mineral groundmass, as indicated by **Figures 7a1** and **7a2**.

- Phenocrysts consisted of plagioclase (40%), pyroxene (7.4%), hornblende (1.4%), and opaque minerals (3.8%). Plagioclase was colourless in PPL and grey in XPL, measuring 0.25–3 mm, prismatic, subhedral, showing albite twinning, and of andesine type. Pyroxene was reddish clear and cream, orange, blue, and purple in XPL. Pleochroic pyroxene, measuring 0.2–1.7 mm, and with a short prismatic shape, subhedral, bidirectional cleavage, moderate darkness, with a darkness angle of 42–45 degrees, had a pyroxene type twin, namely the mineral augite. Hornblende was light brown in PPL and dark brown in XPL. It was pleochroic, measuring 0.8–2.4 mm, and had a long prismatic, subhedral form with 30-degree oblique extinction. Opaque black minerals in PPL and XPL, have crystals sized 0.1–0.7 mm, tabular shape, and euhedral crystal form.
- The groundmass (47.4%) was clear brownish in PPL and dark grey in XPL, present in fine material measuring less than 0.1 mm, short prismatic shape, and consisted of microcrystalline plagioclase.

From the results of mineral identification, we determined that the rock sample was classified as andesite, according to the Quartz, Alkali Feldspar, Plagioclase, Feldspatoid (QAPF) diagram classifying intrusive igneous rocks (**Streckeisen, 1978**).

3.1.2.2. CR2

The second silicate rock sample drilled on Mount Parang was an intrusive body between the Melange Karang Sambung sediment and the Totogan Formation in Kebumen, Central Java. The section under the microscope was identified as a mafic plutonic igneous rock, colourless, colour index 42%, holocrystalline, medium-coarse phaneritic, crystal form, subhedral - anhedral, crystal size 1–5 mm, inequigranular porphyritic, special diabasic texture, composed of plagioclase, sericite, clinopyroxene, and opaque minerals, as indicated by **Figures 7b1** and **7b2**.

The mineral composition consisted of plagioclase (65%), opaque minerals (5%), sericite (5%), and clinopyroxene (25%).

- Colourless plagioclase, low relief, subhedral crystal form, refractive index n mineral > n surrounding mineral, indicating albite mineral twinning. The sample contained phenocrysts measuring approximately 3 mm of labradorite type and microlites about 1 mm in size. Labradorite type was present locally in the section.
- Opaque black mineral, high relief, anhedral crystal form, present locally in the section.
- Sericite appeared as a black mineral with low relief and an anhedral crystal form. It was scattered throughout the section.
- Clinopyroxene was creamy, medium relief, showed two-way cleavage, anhedral crystal form, present locally in the section.

According to the QAPF classification of volcanic rocks for field use (**Streckeisen, 1976**), the sample was Gabbro, i.e. a mafic igneous rock. According to the Classification of Rocks (**Travis, 1955),** the sample was Dolerite, Diabase or Microgabbro.

The silicate rock samples tested had different compositions related to their genesis. Both contained plagio-

Table 2. Summary of characteristics of tested rock samples

CA1	Limestone	Wonosari	Middle Miocene to Pliocene (5–16 million years ago)	3.37±0.19	2.11	21.04	Calcite (60%), Skeletal (30%), Grain aggregate (7%), Opaque mineral (3%)
CA2	Limestone	Sentolo	Early Miocene to Late Miocene (12–22.5 million years ago)	5.91±0.14	2.43	4.44	Calcite (53%), Skeletal (20%), Grain aggregate (20%), Opaque mineral (7%)
CR1	Andesite	Beser	Late Pliocene (1.8–3.6 million years ago)	6.60±0.68	2.90	4.90	Groundmass (47.4%), Plagioclase (40%), Pyroxene (7.4%), Opaque mineral (3.8f%), Hornblende (1.4%)
CR2	Gabbro	Mount Parang	Eocene–Oligocene (26–39 million years ago)	5.64±0.25	2.59	4.43	Plagioclase (65%), Clinopyroxene (25%), Opaque mineral (5%), Sericite (5%)

clase in varying percentages. CR1, andesite, was dominated by groundmass (47%) and plagioclase (40%). CR2, Gabbro, was dominated by plagioclase (65%) and clinopyroxene (25%). Andesite is typically formed as a product of volcanic activity near subduction zones. The cooling process occurred relatively fast and the mineral texture was finer, as indicated by microcrystalline plagioclase in ground mass of CR1 that had fine material measuring less than 0.1 mm. In this ground mass, phenocrysts were distributed with crystal sizes of 0.1–3 mm. CR2, Microgabbro, was formed in intrusive zones at shallow depths. The slower magma cooling process produced larger crystal sizes than andesite. As an indicator, the minerals composing CR2 had crystal sizes of 1–5 mm. Minerals in both silicate samples interlocked to form igneous rocks with high density and velocity. However, the density of CR1 and the velocity of CR2 were reported with more precise data ranges.

Table 2 highlights the characteristics of the tested rock samples to facilitate the analysis of their relationship with changes in rock velocity due to fracture frequency. CA1 and CA2 have similar mineral content (calcite, skeletal, grain aggregate, and opaque minerals) but different percentages. CA1 has a higher content of calcite (60%) and skeletal material (30%) than CA2. CA2 has higher grain aggregate and opaque minerals than CA1, 20% and 7%, respectively. With relatively higher Vp and density, and lower porosity than CA1, CA2 also contains a higher percentage of aggregate grains and opaque minerals. However, the calcite and skeletal content of CA2 is lower than that of CA1. CR1, which has a relatively smaller composition of plagioclase and pyroxene than CR2, has a velocity, density, and porosity slightly higher than CR2. Thus, samples CR1 and CR2 have relatively typical density and velocity. As explained previously by petrography, physical, and dynamical tests, CA1 and CA2 have different velocity, density, and texture, whereas CR1 and CR2 have different mineral content. The genesis, depositional environment, and formation age of the four samples are different. Furthermore, the velocity response of each sample was analysed to the artificial joint treatment with various spacings.

3.2. Empirical equations of fracture frequency and P-wave velocity

Ultrasonic velocity measurements of rock samples with artificial fractures and varying spacing have been conducted in the laboratory on four lithologies. The distribution of P-wave velocity data from the measurement results against fracture frequency is plotted in **Figure 8**. For all lithologies, P-wave velocity decreases with increasing fracture frequency. Based on the data distribution, the decrease is significant in lithologies with high P-wave velocities: CA2, CR1, and CR2. The P-wave velocity of CA1, which has the lowest intact rock velocity, still falls within a range similar to the other three lithologies when the variation in fracture density is approximately more than 10 joints per metre. Evidently, the decrease in P-wave velocity due to the addition of fractures in low-velocity limestone (less than 4 km/s) is not as significant as that in silicate and carbonate rocks that have high velocities (more than 5 km/s).

To quantify the correlation for each lithology, we determined linear trendlines of linear equations between fracture frequency and velocity. These trendlines were used to derive empirical equations to estimate fracture frequency from relative changes in the P-wave velocity of fractured rocks to the velocity of intact rocks.

Figure 9 shows the distribution of P-wave velocity data from laboratory measurements grouped according to lithology. The proposed empirical equations for lithologies CA1, CA2, CR1, and CR2 are $V_{pj}/V_{p0} = 1 - 0.0172FF$, $1 - 0.0301FF$, $1 - 0.0371FF$, and $1 - 0.0349FF$, respectively. V_{pj} is the P-wave velocity of jointed rock, Vp_0 is the P-wave velocity of intact rock, and FF is fracture frequency. Thus, the effect of adding fractures to velocity from the largest to the smallest is in lithologies CR1, CR2, CA2, and CA1, respectively.

Based on the R^2 of the four lithology trendlines, we quantified that the distribution of wave velocity data for the fractured sample CA1 was the most dispersed compared to the other three lithologies. The correlation between fracture frequency and wave velocity was stronger in lithologies with high V_p (more than 5 km/s) and with R^2 above 0.7. Therefore, from our results, using

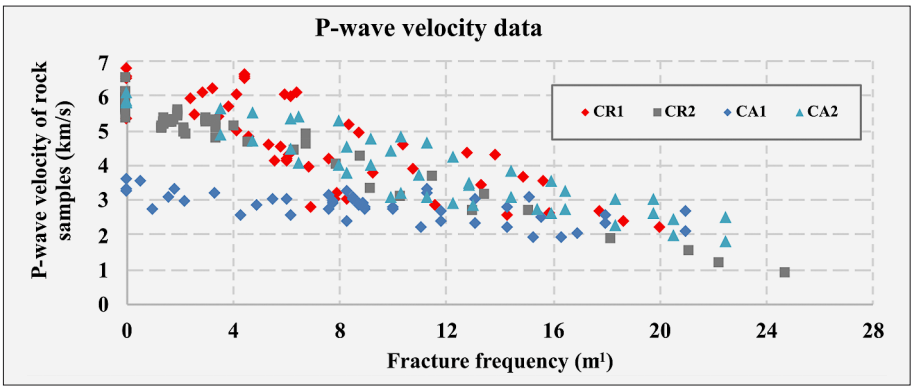

Figure 8. P-wave velocity of the artificial jointed rock sample obtained from ultrasonic velocity measurements in the laboratory. In general, there is a decrease in P-wave velocity for all lithologies. The decrease is significant in lithologies with high P-wave velocities (more than 5 km/s), high density (more than 2.4 g/cm³), and low porosity (less than 5%): CA2, CR1, and CR2. CA1, which has the lowest intact rock velocity (3.71 km/s), lowest density (2.11 g/cm³), and the highest porosity (21.04%), shows the range of Vp that is not much different from the other lithologies when the fracture frequency is approximately more than 10 joints/metre.

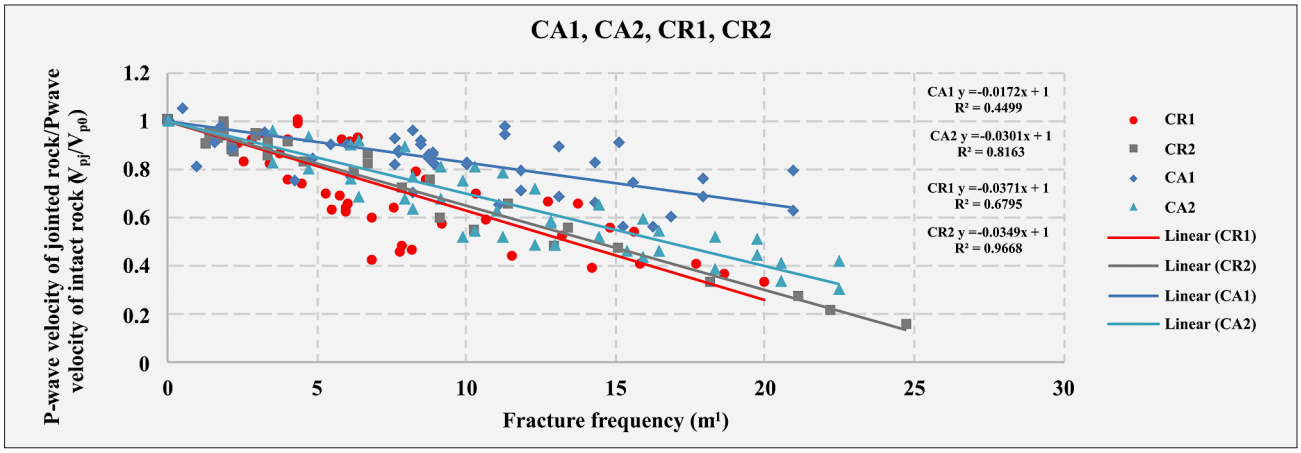

Figure 9. Trendline of velocity data. The ratio of jointed rock velocity to intact rock of CA1 constructs the linear correlation, V_{pj}/V_{po} = 1-0.0172FF, with a coefficient of determination R^2 = 0.4499, classified as a strong correlation. The ratio of jointed rock velocity to intact rock of CA2 constructs the linear correlation, V_{pj}/V_{po} = 1-0.0301FF, with a coefficient of determination R^2 = 0.8136, classified as a very strong correlation. The ratio of jointed rock velocity to intact rock of CR1 constructs the linear correlation, V_{pj}/V_{po} = 1-0.0371FF, with a coefficient of determination R^2 = 0.6795, classified as a very strong correlation. The ratio of jointed rock velocity to intact rock of CR2 constructs the linear correlation, V_{pj}/V_{po} = 1-0.0349FF, with a coefficient of determination R^2 = 0.9688, classified as a very strong correlation.

rock wave velocity values with empirical equations to assist in interpreting or predicting fracture frequencies for rocks with V_p more than 5 km/s is highly recommended. Meanwhile, for carbonate rocks with less compact characteristics, empirical equations can still be used with a lower confidence level.

Subsequently, we grouped the samples into two lithology groups, i.e. carbonate rocks and silicate rocks, as shown in **Figures 10** and **11**. Based on the grouping, the following empirical equations were obtained: for carbonate rocks (CA1 and CA2), $V_{pj}/V_{p0} = 1 - 0.0246FF$, and for silicate rocks (CR1 and CR2), $V_{pj}/V_{p0} = 1 - 0.0361FF$. The decrease in V_p due to the addition of fracture frequency was more significant in silicate rocks than in carbonate rocks, as indicated by the FF multiplier coefficient, i.e. 0.0361 > 0.0246. The carbonate rock data were also more spread out than silicate rocks, with R^2 coefficients of 0.6027 and 0.8520, respectively. However, this does not apply generally to all carbonate rocks. Carbonate rocks with high V_p, such as CA2, showed a more concentrated data distribution on the trendline. The differences in density, porosity, and ultrasonic velocity between CA1 and CA2 affected the variation in the decrease in ultrasonic velocity measurement results in fractured rock samples.

Although the composition of CA1 and CA2 was relatively typical, consisting of calcite, skeletal, grain aggregate, and opaque minerals (listed in **Table 2**), different percentages caused differences in velocity. When considering the level of compaction, CA1, deposited in the Wonosari Formation, is younger than CA2, which was taken from the Sentolo Formation. CA2 was thought

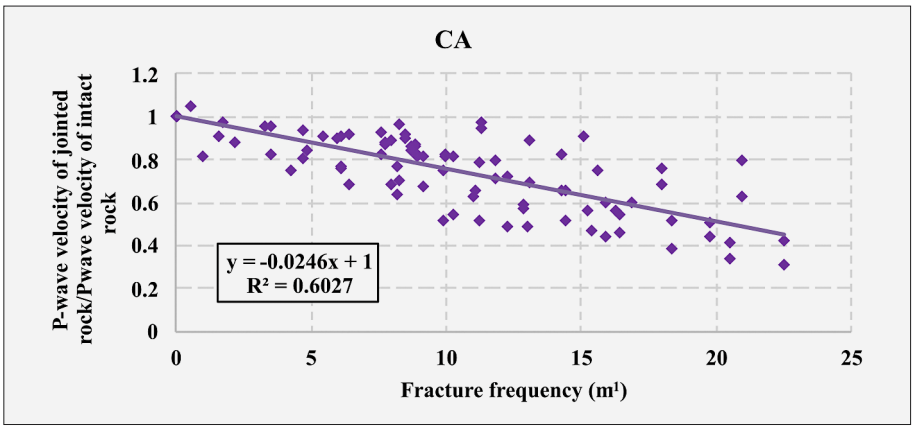

Figure 10. Trendline of velocity data of CA. The ratio of jointed rock velocity to intact rocks constructs the linear correlation, Vp_j/Vp_o = 1-0.0246FF, with a coefficient of determination R^2 = 0.6027, classified as a strong correlation.

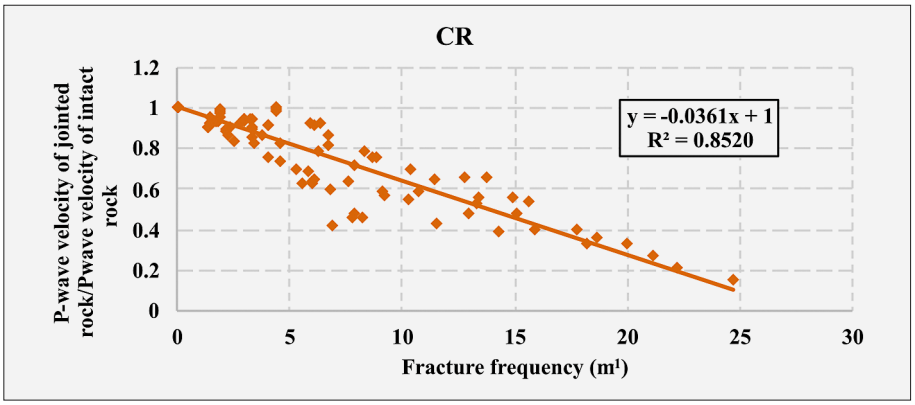

Figure 11. Trendline of velocity data of CR. The ratio of jointed rock velocity to intact rocks constructs the linear correlation, V_{pj}/V_{po} = 1-0.0361FF, with a coefficient of determination R^2 = 0.8520, classified as a very strong correlation.

to have undergone a sedimentation and compaction process over a longer period; thus, its porosity was reduced. CA2 also had relatively higher grain aggregate and opaque minerals than CA1.

The difference in porosity in the silicate rock sample was less significant than in the carbonate rock sample. However, in silicate rocks, porosity also affected the R^2. CR1 had a porosity of 4.90%, and the coefficient of determination was 0.6795 that was lower than CR2, 0.9668, with a porosity of 4.43%. The density, porosity, and ultrasonic velocity differences between CR1 and CR2 were less significant than between the carbonate rock samples. Therefore, besides the fracture frequency having a more significant influence on rock velocity, the confidence level in predictions in silicate rocks would be higher than in carbonate rocks because the properties of carbonate rocks were more heterogeneous.

We also provided a general equation for all lithologies of the samples measured in this study (see **Figure 12**). Obviously, carbonate rocks were partly located above the data distribution area, and silicate rocks were concentrated in the lower area of the data distribution. The proposed empirical equation, $V_{pj}/V_{p0} = 1 - 0.0271FF$, can predict fracture frequency from wave velocity for various rock types.

The relationship equation between ultrasonic velocity and fracture frequency has been quantified as a result of the study. An example of its application is for preliminary exploration when the scope of the study area is regional. The equation can be employed to obtain an overview of the distribution of rock mass quality through fracture frequency prediction. We believe that the equation obtained from this study can be applied on various types of other carbonate or silicate rocks because the velocity parameter in these equations is expressed as a ratio, between the V_p of fractured rocks and the V_p of the intact rock itself. The increase in fracture frequency has an impact on the decrease in velocity and also depends on the intact rock's velocity. The intact rock's velocity itself will produce the prediction results of our equations that applies specifically to certain rocks, which makes it relevant for direct use on rocks from other sites. Notably, the prediction uncertainty is inherently linked to the intact velocity of the measured rock. Rocks with low intact velocities are more sensitive to changes in V_p due to the presence of fractures. An example is clearly seen in

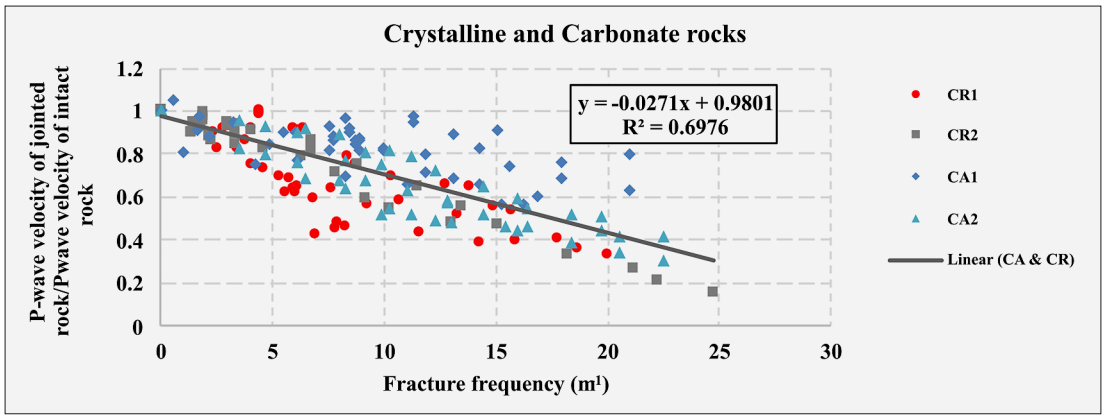

Figure 12. Trendline of velocity data of CR and CA. The ratio of jointed rock velocity to intact rocks constructs the linear correlation, V_{pj}/V_{po} = 1-0.0271FF, with a coefficient of determination R^2 = 0.6976, classified as a strong correlation.

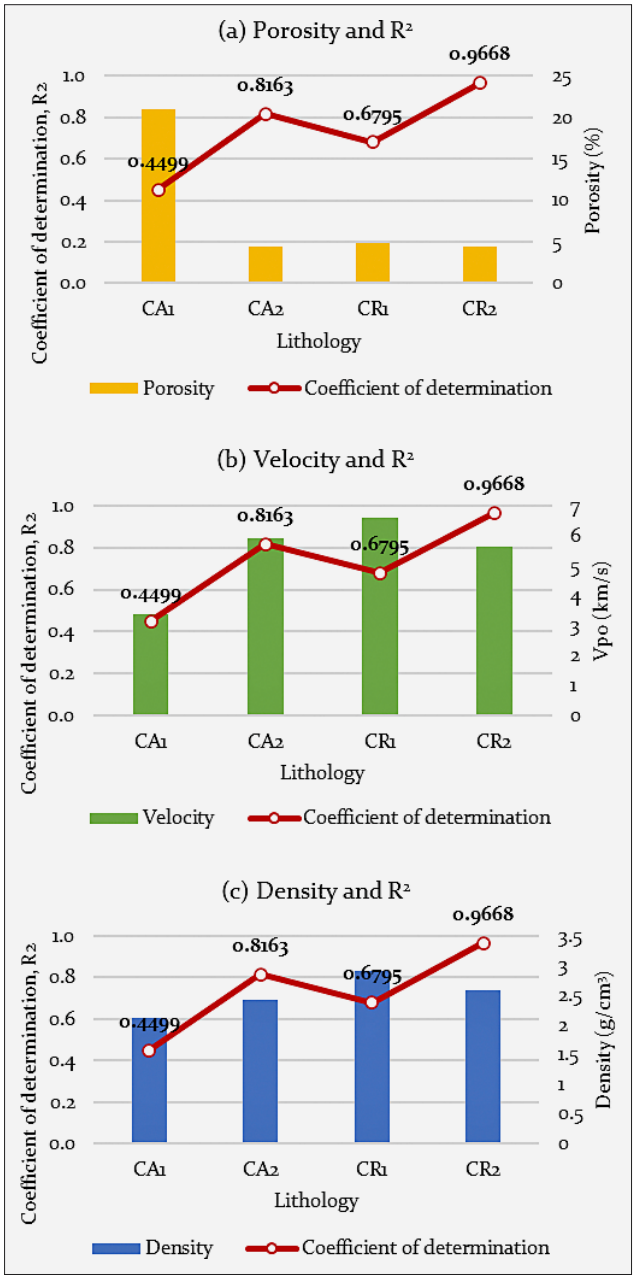

CA1, which has a velocity of less than 4 km/s. The range of data variance along the linear trend line is relatively more spread out, thus the equation we obtained is very helpful for rocks with high velocities (>5 km/s) and requires attention for rocks with low velocities (<4 km/s).

We also plotted the coefficient of determination against the porosity, velocity, and density of each lithology to analyse the physical properties and characteristics against the prediction accuracy of the constructed equation. Through the visualisation in **Figure 13**, we can conclude that, generally, R^2 is highly determined by porosity, velocity, and density. The effects were characterized specifically for carbonate and silicate rock lithology.

In terms of petrography, CA1 has a higher percentage of calcite and skeletal than CA2. CA1 has a lower density and velocity than CA2. The porosity of CA1 is also relatively lower. The range of velocity, density, and porosity data for CA1 is wider than CA2. Thus, for these carbonate rock samples CA1 and CA2, the difference in R^2 is largely determined by the density of the sample grains. A denser and more compact sample with a narrower data range, CA2, provides better R^2.

CR1 has a higher velocity than CR2 with a wider range. The density and porosity are relatively equivalent. Relatively, the difference in values and ranges of CR1 and CR2 properties is not as significant as between CA1 and CA2. Therefore, the difference in velocity does affect not clearly on the difference in R2 in silicate rock

Figure 13. A combined plot shows the correlation between determination and properties of rocks. (a) The coefficient of determination tends to be negatively related to porosity. A high porosity sample (CA1) has a lower coefficient of determination than a low porosity sample (CA2, CR1, and CR2). (b) The determination coefficient is positively related to velocity. Low-velocity samples (CA1) have a lower coefficient of determination than high-density samples (CA2, CR1, and CR2). (c) The determination coefficient is positively related to density. Low-density samples (CA1) have a lower coefficient of determination than high-density samples (CA2, CR1, and CR2).

Table 3. Summary of empirical equations relating to the fracture frequency (FF), P-wave velocity of intact rock (V_{po}), P-wave velocity of jointed rock (V_{pj}), and their coefficient of determination (R^2)

No.	Lithology	Empirical equation of FF and Vp	(R^2)
1	CA1 (Wonosari Limestone)	$V_{pj}/V_{p0} = 1 - 0.0172FF$	0.4499
2	CA2 (Sentolo Limestone)	$V_{pj}/V_{p0} = 1 - 0.0301FF$	0.8163
3	CR1 (Beser andesite)	$V_{pj}/V_{p0} = 1 - 0.0371FF$	0.6795
4	CR2 (Mount Parang Gabbro)	$V_{pj}/V_{p0} = 1 - 0.0349FF$	0.9668
5	Carbonate rocks (CA1 & CA2)	$V_{pj}/V_{p0} = 1 - 0.0246FF$	0.6027
6	Silicate rocks (CR1 & CR2)	$V_{pj}/V_{p0} = 1 - 0.0361FF$	0.8520
7	Carbonate and silicate rocks (CA1, CA2, CR1, CR2)	$V_{pj}/V_{p0} = 1 - 0.0271FF$	0.6976

samples since the samples are relatively typical. In this silicate rock, the mineral composition and the rock genesis are expected to play a greater role in the difference in R^2. CR1 is a volcanic rock, while CR2 is a plutonic rock. According to its petrography, CR1 is relatively more heterogeneous than CR2 because CR1 is composed of matrix minerals embedded in the ground mass. Meanwhile, CR2 is an intrusive body and composed of interlocked minerals.

Thus, we conclude that the R^2 in carbonate rocks and silicate rocks is determined by different parameters. In carbonate rocks, differences in R^2 are largely influenced by factors related to density (including velocity and porosity). Meanwhile, the difference in R^2 in silicate rocks is defined by the genesis of the rock, which affects the heterogeneity of its minerals. In addition, when viewed from the age of the formation (age information is listed in **Table 2**), there is a similar pattern between carbonate rocks and silicate rocks. CA2 and CR2 that have higher R^2 are older formations than CA1 and CR1. Earlier-formed rocks experienced more historical stress than later-formed rocks. Thus, the compaction factor is also considered to play a role in determining R^2 of all samples.

The equations produced in this study include a wider range of fracture frequency with considerable data. The constructed equations (listed in **Table 3**) complement previous studies' results that conducted the measurements on rock samples with tight joint spacing and limited data (less than 10 data) on marble, calcarenite, and gypsum samples (**Kurtulus et al., 2012; Huang et al., 2014; Leucci and De Giorgi, 2006; Varma et al., 2017; Sarglou and Kallimogiannis, 2017**). The results of this study emphasised that the presence of joints in rocks reduced the wave propagation velocity. The shorter the joint space in the measured sample, the lower the P-wave velocity is, forming a linear equation trend. The correlation between fracture frequency and the obtained velocity is classified as strong to very strong; this is indicated by the determination coefficient of all equations being more than 0.45 - 0.97. The fracture frequency can explain the variance of the velocity ratio (V_{pj}/V_{p0}); thus, these equations will be reliable for estimating fracture frequency at sites. The range of fracture frequency of rock samples measured in this study, namely 0-24 joints per metre, is wider in scope than published laboratory measurements.

Based on a correlation study between velocity with fracture frequency and RQD at several sites against eight lithologies, **Sjogren et al. (2006)** found that the prediction accuracy increased if the more competent rock mass was also considered. **Boadu (1997)** found that low velocity in seismic measurements in the field were associated with fractured zones. In this study, the measured samples represented competent rocks in the field, with a fracture frequency of less than 10 joints per metre and fractured rocks up to 24 joints per metre. With a larger amount of data (170 data) conducted in this study and an analysis that considers the sample characteristics of carbonate and silicate lithology, the equations from this study show high confidence in terms of R^2 and cover a wide range of fracture frequency in estimating fractures from P-wave velocity.

4. Conclusions

In this study, the effect of fracture frequency on seismic velocity has been examined through ultrasonic velocity measurements in the laboratory for various fracture frequencies and lithologies. Artificial joints were added to the rock drill core using a diamond rock cutter to create fractured rock models with various joint spacings. We successfully created an empirical equation that related the ratio of fractured rock velocity to intact rock velocity (Vp_j/Vp_0) and fracture frequency. The differences in physical and dynamic properties affected the correlation, while a strong correlation between V_p and fracture frequency was found in silicate rocks. Rock compaction in carbonate rocks (indicated by porosity) was assumed to affect the dispersion of the data and the degree of influence of the fracture frequency on V_p. The CA1 data with less compact characteristics (indicated by the high porosity, low velocity, and low density) showed a more dispersed decrease in the V_p pattern. Thus, the empirical equation for interpreting fracture frequency from seismic velocity for silicate and carbonate rocks with V_p higher than 5 km/s and porosity lower than 5% had a higher confidence level than carbonate rocks with low V_p and porosity greater than 20%. The equations ob-

tained in this study showed high confidence in terms of R^2. Therefore, the study findings may be useful in interpreting on-site seismic exploration data in areas with lithology contrast, for example, at the contact boundary of carbonate and silicate rocks or on rocks with different compaction levels.

Acknowledgement

We would like to express our gratitude to the researchers in our Geomechanics - Mining Engineering and Global Geophysics groups. Their invaluable knowledge and competence assisted us in undertaking this new research topic. We also appreciate the assistance of the staff and technicians at the Geomechanics and Mining Equipment Laboratory, Vulcanology and Geothermal Laboratory, and Geophysical Instrumentation and Electronics Laboratory in providing us with the resources needed to conduct the research.

This research was supported by funds from the Centre for Education Services (Pusat Layanan Pendidikan) under the Ministry of Education, Culture, Research, and Technology of the Republic of Indonesia and Indonesia Endowment Fund for Education Agency (LPDP) awarded to Sari Melati (grant number: 202101122085), *Riset Unggulan* of ITB awarded to Ridho K. Wattimena, *Program Penguatan Riset dan Inovasi* of ITB awarded to David P. Sahara, and *Revitalisasi Peralatan Laboratorium* of ITB awarded to Ganda M. Simangunsong.

5. References

Ahr, W. M. (2011). Geology of carbonate reservoirs: the identification, description and characterization of hydrocarbon reservoirs in carbonate rocks. John Wiley & Sons, 296 p.

Akmaluddin, A. and Agustin, M. V. (2019). Stratigraphy and Foraminiferal biostratigraphy of Sentolo formation in Sedayu Area: Local Unconformity Identification in Early Pliocene. Journal of Applied Geology, 3(2), 32-47.

Asikin, S., Handoyo, A., Busuno H. and Gafoer, S. (1992). Geological Map of the Kebumen Quadrangle, Jawa. Systematic Geological Map, Indonesia. Quadrangle: Kebumen-1401-1. Geological Research and Development Centre of Indonesia.

Boadu, F. K. and Long, L. T. (1996). Effects of fractures on seismic-wave velocity and attenuation. Geophysical Journal International, 127(1), 86-110.

Brannon, C., Beard, D., Pascoe, N. and Priatna, A. (2020). Development of and production update for the Grasberg Block Cave mine–PT Freeport Indonesia. In: MassMin 2020: Proceedings of the Eighth International Conference & Exhibition on Mass Mining, University of Chile, 747-760.

Cai, W., Dou, L., Cao, A., Gong, S. and Li, Z. (2014). Application of seismic velocity tomography in underground coal mines: a case study of Yima mining area, Henan, China. Journal of Applied Geophysics, 109, 140-149.

Córdova, E., Gottreux, I., Anani, A., Ferrada, A. and Contreras, J. S. (2021). Blasting and preconditioning modelling in underground cave mines under high stress conditions. Journal of the Southern African Institute of Mining and Metallurgy, 121(2), 71-80.

Dugdale, A. L., Wilson, C. J., Leader, L. D., Robinson, J. A. and Dugdale, L. J. (2009). Carbonate spots: Understanding the relationship to gold mineralization in central Victoria, southeastern Australia. Mineralium Deposita, 44, 205-219.

Dunham, R.L. (1962). Classification of carbonate rocks according to depositional texture. Memoir American Association Petroleum Geology Bulletin, 19, 730-781.

Folk, R.L. (1959). Practical petrographic classification of limestones. Bulletin American Association Petroleum Geologists, 43, 1-38.

Gumede, H. and Stacey, T. R. (2007). Measurement of typical joint characteristics in South African gold mines and the use of these characteristics in the prediction of rock falls. Journal of the Southern African Institute of Mining and Metallurgy, 107(5), 335-344.

Haryanto, I. and Sudjradjat, A. (2018). On the Geomorphology and Tectonic Position of Ciletuh-Jampang Area, West Java, Indonesia. Universal Journal of Geoscience, 6(2), 47-54.

He, M., Zhang, Z. and Li, N. (2021). Prediction of fracture frequency and RQD for the fractured rock mass using drilling logging data. Bulletin of Engineering Geology and the Environment, 80, 4547-4557.

Hidayat, W., Sahara, D.P., Widiyantoro, S., Suharsono, S., Riyanto, E., Nukman, M., Wattimena, R.K., Melati, S., Sitorus, E., Nainggolan, T. and Putra, I.P.R.A. (2024). 4D time lapse tomography for monitoring cave propagation and stress distribution in Deep Mill Level Zone (DMLZ) PT Freeport Indonesia. Geomechanics and Geophysics for Geo-Energy and Geo-Resources, 10(1), 39.

Higgs, N. B. (1984). The Profile-Area and Fracture-Frequency Methods: Two Quantitative Procedures for Evaluating Fracture Spacing in Drill Core. Bulletin of the Association of Engineering Geologists, 21(3), 377-386.

Huang, X., Qi, S., Guo, S. and Dong, W. (2014). Experimental study of ultrasonic waves propagating through a rock mass with a single joint and multiple parallel joints. Rock Mechanics and Rock Engineering, 47, 549-559.

Khorzoughi, M. B., Hall, R. and Apel, D. (2018). Rock fracture density characterization using measurement while drilling (MWD) techniques. International Journal of Mining Science and Technology, 28, 6, 859-864.

Kim, J. and Song, J. J. (2019). Scanline based metric for evaluating the accuracy of automatic fracture survey methods. Tunnel and Underground Space, 29(4), 230-242.

Kurtuluş, C., Üçkardeş, M., Sarı, U. and Onur Güner, Ş. (2012). Experimental studies in wave propagation across a jointed rock mass. Bulletin of Engineering Geology and the Environment, 71, 231-234.

Laubscher, D. H. (1990). A geomechanics classification system for the rating of rock mass in mine design. Journal of the Southern African Institute of Mining and Metallurgy, 90(10), 257-273.

Lee Rodgers, J. and Nicewander, W. A. (1988). Thirteen ways to look at the correlation coefficient. The American Statistician, 42(1), 59-66.

Leucci, G. and De Giorgi, L. (2006). Experimental studies on the effects of fracture on the P and S wave velocity propa-

gation in sedimentary rock ("Calcarenite del Salento"). Engineering Geology, 84(3-4), 130-142.

Mandrone, G. (2006). Engineering geological mapping of heterogeneous rock masses in the Northern Apennines: an example from the Parma Valley (Italy). Bulletin of Engineering Geology and the Environment, 65, 245-252.

Mareta, N., Anshori, C. and Hidayat, E. (2020). Geosite and Geomorphosite Assesment of Parang Hill for Geotourism Development and Spatial Planning in Karangsambung-Karangbolong National Geopark. In: International Conference on Regional Development 1, 1, 111-121.

Marinos, V., Goricki, A. and Malandrakis, E. (2019). Determining the principles of tunnel support based on the engineering geological behaviour types: example of a tunnel in tectonically disturbed heterogeneous rock in Serbia. Bulletin of Engineering Geology and the Environment, 78, 4, 2887-2902.

Martyushev, D. A., Yang, Y., Kazemzadeh, Y., Wang, D. and Li, Y. (2024). Understanding the mechanism of hydraulic fracturing in naturally fractured carbonate reservoirs: Microseismic monitoring and well testing. Arabian Journal for Science and Engineering, 49(6), 8573-8586.

Matula, M. (1969). Engineering geologic investigations of rock heterogeneity. In: 11th US Symposium on Rock Mechanics, 25-42.

Moos, D. and Zoback, M. D. (1983). In situ studies of velocity in fractured crystalline rocks. Journal of Geophysical Research: Solid Earth, 88(B3), 2345-2358.

Panek, L. A. (1984). Interpretation of fracturing in drill cores. In 25th US Symposium on Rock Mechanics, P503-510.

Pollard, P. J., Taylor, R. G. and Peters, L. (2005). Ages of intrusion, alteration, and mineralization at the Grasberg Cu-Au deposit, Papua, Indonesia. Economic Geology, 100(5), 1005-1020.

Priest, S. D. (2004). Determination of discontinuity size distributions from scanline data. Rock Mechanics and Rock Engineering, 37, 347-368.

Qian, J., Zhang, H. and Westman, E. (2018). New time-lapse seismic tomographic scheme based on double-difference tomography and its application in monitoring temporal velocity variations caused by underground coal mining. Geophysical Journal International, 215(3), 2093-2104.

Koesmono, M., Kusnama and Suwarna N. (1996). Geological Map of the Sindangbarang and Bandarwaru Quadrangle, Jawa. Systematic Geological Map, Indonesia. Quadrangle: Sindang barang dan Bandarwaru-1208-2 & 1208-5. Geological Research and Development Centre of Indonesia.

Rahardjo, W., Sukandarrumidi and Rosidi, H.M.D. (1995). Geological Map of the Yogyakarta Sheet, Jawa. Systematic Geological Map, Indonesia. Sheet: Yogyakarta-1408-2 & 1407-5. Geological Research and Development Centre of Indonesia.

Rahmouni, A., Boulanouar, A., Boukalouch, M., Géraud, Y., Samaouali, A., Harnafi, M. and Sebbani, J. (2013). Prediction of porosity and density of calcarenite rocks from P-wave velocity measurements. International Journal of Geosciences, 4, 1292-1299.

Saha, K. and Sebastian, R. (2023). Dynamic behaviour of rock joint during shear wave propagation: The influence of joint orientation. Rock Mechanics and Rock Engineering, 56(12), 9203-9213.

Samodra, H., Gafoer, S. and Tjokrosaputro, S. (1992). Geological Map of the Pacitan Quadrangle, Jawa. Systematic Geological Map, Indonesia. Quadrangle: Pacitan-1507-4. Geological Research and Development Centre of Indonesia.

Saroglou, C. and Kallimogiannis, V. (2017). Fracturing process and effect of fracturing degree on wave velocity of a crystalline rock. Journal of Rock Mechanics and Geotechnical Engineering, 9(5), 797-806.

Şen, Z. (2014). Rock quality designation-fracture intensity index method for geomechanical classification. Arabian Journal of Geosciences, 7, 2915-2922.

Şen, Z. and Sadagah, B. H. (2003). Modified rock mass classification system by continuous rating. Engineering Geology, 67(3-4), 269-280.

Sjogren, B., Ofsthus, A. and Sandberg, J. (1979). Seismic classification of rock mass qualities. Geophysical Prospecting, 27(2), 409-442.

Sriwidada, B. W. and Kurnia, A. A. (2017). Joint Rock observation at mine underground face mapping at pongkor gold mining business unit, PT. ANTAM., Tbk. Joint Convention Malang 2017, HAGI – IAGI – IAFMI – IATMI (JCM 2017).

Streckeisen, A. (1976). Plutonic rocks. Classification and nomenclature recommended by the IUGS-Subcommission on the Systematic of Igneous Rocks. Geotimes, 18, 26-36.

Taraldsen, G. (2021). Confidence in Correlation. Technical Repository, 1-9.

Travis, R.B. (1955). Classification of Rocks. Colorado School of Mines, 98 p.

Ulussay, R. (2015). The ISRM Suggested Methods for Rock Characterization, Testing and Monitoring: 2007–2014. Springer, 293 p.

Varma, M., Maji, V. B. and Boominathan, A. (2021). Influence of rock joints on longitudinal wave velocity using experimental and numerical techniques. International Journal of Rock Mechanics and Mining Sciences, 141, 104699.

Varma, M., Maji, V.B. and Boominathan, A. (2017). A study on ultrasonic wave propagation across fractures in jointed rocks. In 51st US Symposium on Rock Mechanics

Verstappen, H. T. (2010). Indonesian landforms and plate tectonics. Indonesian Journal on Geoscience, 5(3), 197-207.

Voudouris, P., Melfos, V., Spry, P. G., Bonsall, T. A., Tarkian, M. and Solomos, C. (2008). Carbonate-replacement Pb–Zn–Ag±Au mineralization in the Kamariza area, Lavrion, Greece: Mineralogy and thermochemical conditions of formation. Mineralogy and Petrology, 94, 85-106.

Wang, Z., Li, X., Zhao, D., Shang, X. and Dong, L. (2018). Time-lapse seismic tomography of an underground mining zone. International Journal of Rock Mechanics and Mining Sciences, 107, 136-149.

Wibowo, N. B., Fathani, T. F., Pramumijoyo, S. and Marliyani, G. I. (2023). Microzonation of seismic parameters in geological formation units along the Opak River using microtremor measurements. Geomate Journal, 25(110), 208-219.

Zhou, X., Jiao, W., Han, J., Zhang, J., Yu, H. and Wu, L. (2010). Tracing hydrocarbons migration pathway in carbonate rock in Lunnan-Tahe oilfield. Energy Exploration & Exploitation, 28(4), 259-277.

SAŽETAK

Empirijska jednadžba procjene učestalosti pukotina karbonatnih i silikatnih stijena pomoću određivanja brzine prolaska P-valova

Frekvencija pukotina (*fracture frequency* FF) nužna je za kvantifikaciju pukotina pri klasifikaciji stijenske mase i znatno utječe na mehanička svojstva stijenske mase. U prošlosti su laboratorijska istraživanja o učincima raspucanosti stijena na brzinu prolaza ultrazvučnih valova kroz stijene bile usmjerene na uvjete visokoga FF-a te nisu uključivale litološke razlike. Cilj je ovoga rada procijeniti FF na temelju određivanja njegova odnosa s brzinom prolaza ultrazvučnih valova u karbonatnim i silikatnim stijenama. Dvije karbonatne (CA1 i CA2) i dvije silikatne (CR1 i CR2) stijene uzorkovane su na četirima lokacijama na otoku Javi u Indoneziji. Njihove su karakteristike određene na temelju petrografskih analiza, određivanjem fizičkih svojstava i ispitivanjem brzine prolaza ultrazvučnih valova. U uzorcima tih stijena napravljene su umjetne pukotine kako bi se stvorio različit razmak pukotina, posebno na niskim frekvencijama između 0 i 24 pukotine po metru. Napravljene su nove empirijske jednadžbe koje izražavaju odnos između FF-a, brzine prolaza P-valova kroz intaktne stijene (Vp_o) i brzine prolaza P-vala kroz raspucale stijene (Vp_j). Omjeri Vp_j/Vp_o bili su za CA1 1–0,0172FF, za CA2 1–0,0301FF, za CR1 1–0,0371FF i za CR2 1–0,0349FF. Koeficijent determinacije jednadžbe za svaki varijetet pokazao je da su poroznost, brzina i gustoća utjecali na podatke u jednadžbi. Zaključeno je da se rezultati ovoga rada mogu koristiti za optimizaciju korištenja geofizičkih metoda za geotehničko praćenje, posebno za identifikaciju FF-a u litološkome kontrastu između karbonatnih i silikatnih stijena ili stijena s različitim razinama kompaktnosti.

Ključne riječi:
karbonati, silikatne stijene, frekvencija pukotina, ultrazvučno mjerenje, brzina vala u stijeni

Author's contribution

Sari Melati conducted the laboratory measurement, performed data processing, and wrote the paper. **Ridho K. Wattimena**, **David P. Sahara**, and **Ganda M. Simangunsong** shared resources in their research groups to conduct this study. **Wahyu Hidayat** supported the sample provision and data acquisition.
All authors have read and agreed to the published version of the manuscript.